ACS Sustainable Chemistry & Engineering

pubs.acs.org/journal/ascecg

Research Article

Direct Z-Scheme Tannin–TiO_2 Heterostructure for Photocatalytic Gold Ion Recovery from Electronic Waste

Kyeong Rak Kim, Saehan Choi, Cafer T. Yavuz, and Yoon Sung Nam*

Cite This: *ACS Sustainable Chem. Eng.* 2020, 8, 7359–7370

Read Online

ACCESS | Metrics & More | Article Recommendations | Supporting Information

ABSTRACT: Precious-metal recovery from industrial wastewater has received considerable attention because of rapidly increasing amounts of electronic waste. Existing technologies have yet to be widely applied due to their high cost and low selectivity toward precious-metal ions. Herein, we report a direct Z-scheme tannin–TiO_2 heterostructure for selective gold adsorption from electronic waste under solar irradiation. The tannin-coated TiO_2 nanoparticles were prepared by a simple dipping method, and under light illumination, both tannin and TiO_2 can serve as photosensitive components for the reduction of metal ions, with metal-to-ligand charge transfer from TiO_2 to tannin extending the lifetime of the excited electrons. Moreover, no additional electron donors are required because the tannin layer scavenges the reactive oxygen species generated by the holes from the light-activated TiO_2 surface. The heterostructure allows for the highly efficient photocatalytic recovery of gold ions, with 11 times higher adsorption capacity in the light compared to the dark. High selectivity toward gold ions was also demonstrated using a metal ion mixture including nine different metal ions that are commonly found in electronic waste. Our findings suggest that the Z-scheme heterostructure of polyphenol and semiconductor provides a promising photochemical pathway for efficient and selective metal ion recovery from electronic waste.

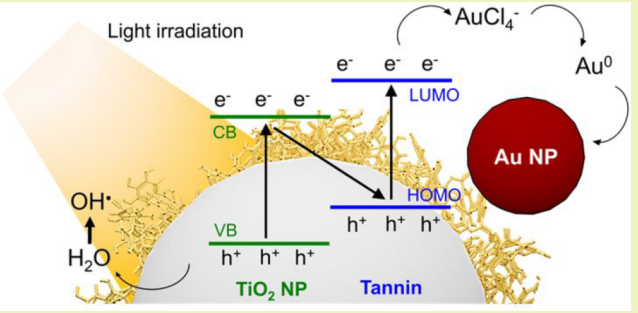

KEYWORDS: *Titanium dioxide, Tannin, Gold nanoparticles, Electronic waste, Metal recovery*

INTRODUCTION

Metal recovery from industrial wastewater has recently received much attention, particularly regarding the recycling of precious metals and the prevention of hazardous heavy-metals emission.[1] For example, precious-metal recovery from electronic waste (E-waste) has been termed "urban mining" and aims to recover precious metals that have accumulated in industrial wastes. It is more efficient than natural mining, especially when considering the rapid increase in E-waste.[2] Among the precious metals found in E-waste, gold attracts significant attention due to its wide range of practical uses and high economic value.[3] Current industrial processes heavily depend on pyrometallurgy, which involves the thermal treatment of E-waste for recovery of valuable metals.[4] However, this method is highly energy intensive because it relies on fossil fuel, thus resulting in high operation costs and additional environmental problems, such as discharge of organic chemicals. Hydrometallurgy, involving chemical reduction and electrowinning, is a good alternative to pyrometallurgy for metal recovery because it is cost-effective and has a low environmental impact. However, it is limited by the excessive loss of organic solvents and chemical reagents used during the separation processes. For sustainable metal recovery, adsorption exhibits energy efficiency and high selectivity toward the target metal, and its long-term application causes low levels of environmental pollution. Therefore, adsorption is currently considered as an ecofriendly and inexpensive method for selective metal recovery, because it can be conducted without the use of additional reagents.[5] Although numerous adsorbents have been investigated, including biological adsorbents, activated carbon, and surface-functionalized porous substrates,[6−10] their performance has been evaluated only using dilute gold solutions. Gold adsorption capacity and selectivity toward gold ions have not been widely investigated for industrial applications.

For the development of sustainable and ecofriendly systems, bioinspired adhesive materials have been investigated as multifunctional coatings for a variety of substrates.[11−13] They can also attract metal ions from aqueous solutions efficiently and easily produce metal–organic hybrid structures.[14−18] For example, polyphenols can act as metal ion reducing agents

Received: February 5, 2020
Revised: April 1, 2020
Published: April 23, 2020

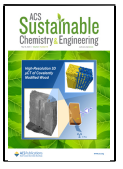

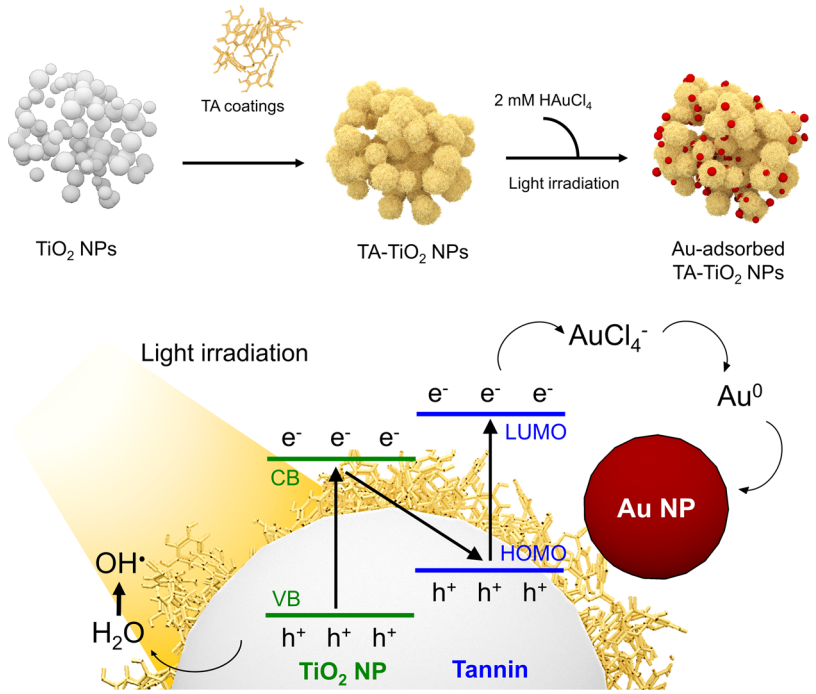

Figure 1. Schematic procedures of gold adsorption using tannin-coated TiO_2 nanoparticles under light irradiation.

(e.g., gold, silver, and palladium), with the phenolic groups being oxidized to quinones while electrons are transferred to the metal precursors, allowing for the generation of metal nanostructures. The common polyphenol groups, galloyl and catechol, have redox potentials of 0.897 and 0.530 V, respectively, which are slightly lower than the reduction potential of $AuCl_4^-$($AuCl_4^- + 3e^- = Au^0 + 4Cl^-$, $E^0 = 1.002$ V).[19,20] Under light irradiation, catechol becomes quinone while releasing a proton−electron pair, and the released proton can be transferred to a neighboring substance.[21,22] When excited under light illumination, tetrachloroaurate ions ($AuCl_4^-$) can become unstable via ligand-to-metal charge transfer (LMCT) and dissociate into auric trichloride ($AuCl_3^-$) and a radical chlorine, which quickly recombine to re-form $AuCl_4^-$.[23] However, in the presence of tannin (TA) as a proton donor, the radical chloride is reduced to a chloride ion and $AuCl_3^-$ is subsequently reduced to metallic gold. Moreover, once gold nanoparticles (AuNPs) are formed on the TA surface, localized surface plasmon resonance (LSPR) causes them to extend light absorption from UV light to visible or near-infrared (NIR) light.[24] LSPR excitation can generate hot carriers, which can serve as a driving force for chemical reactions and the formation of nanocrystals.[25,26]

Our recent work demonstrated that the photochemical activation of TA-coated polymer microspheres can facilitate the adsorption of metal ions.[27] However, the photochemical activity of TA was measured on an inert polymer substrate. This single-component photochemical reaction has limitations, such as undesirable backward reactions and reduction of light absorption by redox mediators. By changing the substrate to a photosensitive alternative, TA can be photochemically activated further to avoid the limitations of the single-component reaction. Therefore, heterogeneous semiconductors can be considered as substrates for TA, instead of polymer microspheres, to control charge transfer and broaden the light absorption spectrum, which should facilitate the adsorption of metal ions.[28,29]

There have been extensive studies of photocatalytic reactions on semiconductor surfaces, particularly using titanium dioxide (TiO_2) due to its low cost, nontoxicity, and high photochemical stability.[30,31] Photocatalytic activities and reaction mechanisms rely on the transfer of photoinduced charges to the surface. Therefore, various methods have been applied to improve the photocatalytic activities of TiO_2, such as metal deposition,[24] anion complexation,[32] and polymer coatings;[33] for example, polyphenolic compounds are known to form ligand-to-metal charge transfer (LMCT) complexes on TiO_2.[22,32] This allows direct Z-scheme heterojunctions to be constructed as an effective means of overcoming the drawbacks of single-component photochemical reaction.[34] TA-coated TiO_2 nanoparticles (denoted as "TA−TiO_2 NPs") were studied for sunblock applications because of the increased UV light absorption through LMCT and the reactive oxygen species (ROS) scavenging activity of TA.[31] However, no study has been reported for gold ion recovery using TA−TiO_2 NPs through the direct Z-scheme mechanism.

In this work, we introduce a direct Z-scheme heterojunction based on TA−TiO_2 NPs to selectively enhance the gold adsorption on TA layers under light illumination (Figure 1). TiO_2 NPs were used as a stable and photosensitive substrate, as previously reported.[30,31] The surfaces of the TiO_2 NPs were coated with TA using a simple dipping method. Interestingly, the synergistic effect of TA and the TiO_2 NPs was driven by a direct Z-scheme mechanism, and so the maximum amount of gold ions adsorbed under 1-sun irradiation was effectively increased. The photoenhanced adsorption of gold ions was investigated using adsorption kinetics and isotherm models. The metal selectivity of the TA−TiO_2 NPs was also investigated using nine different metal chlorides.

RESULTS AND DISCUSSION

Preparation and Characteristics of Tannin-Coated TiO_2 Nanoparticles. TA−TiO_2 NPs were prepared by a

https://dx.doi.org/10.1021/acssuschemeng.0c00860
ACS Sustainable Chem. Eng. 2020, 8, 7359−7370

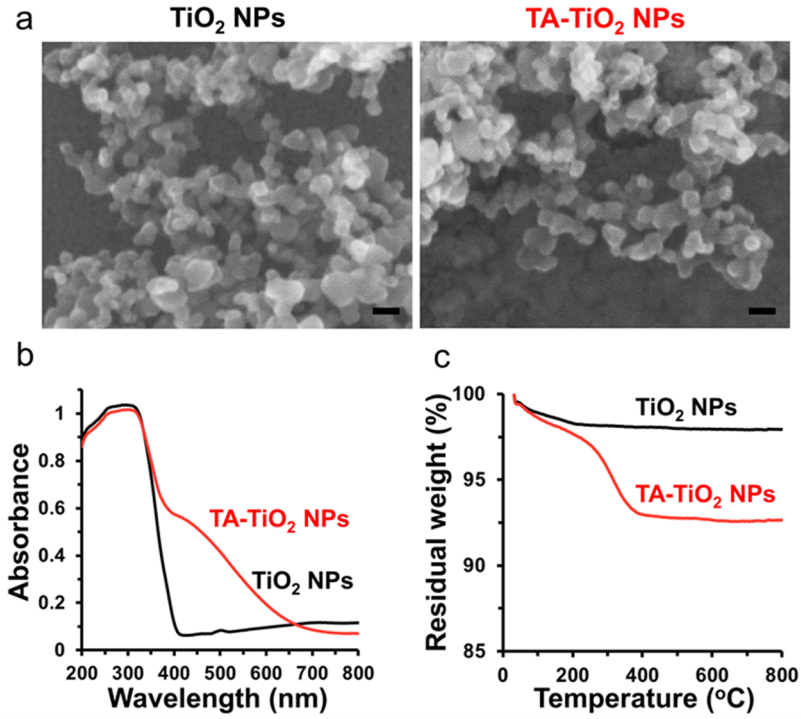

Figure 2. Characteristics of TiO_2 NPs and TA-coated TiO_2 NPs. SEM images (scale bar: 40 nm) (a), UV−vis absorption spectra (b), and TGA diagram (c) of TiO_2 and TA−TiO_2 NPs.

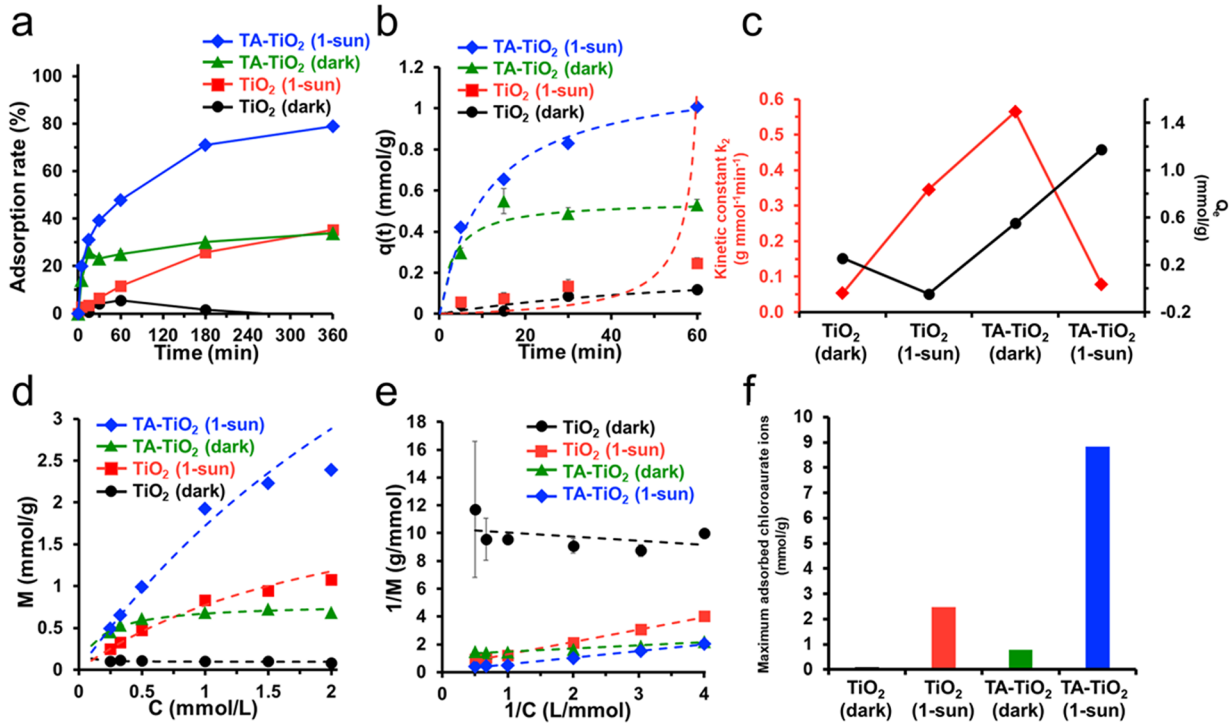

Figure 3. Gold adsorption kinetics (a), pseudo-second-order kinetics plots (b), the number of adsorbed gold ions on adsorbent at equilibrium and the kinetic constant (c), Langmuir isotherm curves (d), Lineweaver−Burk plots (e), and the maximum amounts of adsorbed gold ions on adsorbents and the Langmuir constant (f) for gold ion adsorption on TiO_2 and TA−TiO_2 NPs. Symbols represent the mean and standard deviation (n = 5).

simple dipping method. In brief, a TA solution (10 mg mL^{-1}) was added to a TiO_2 dispersion (100 mg mL^{-1}), and the mixture was stirred magnetically at 300 rpm and 25 °C for 1 h. After being washed several times, the TA−TiO_2 NPs were dried under vacuum at 25 °C. Scanning electron microscopy (SEM) images of pristine TiO_2 nanoparticles (TiO_2 NPs) and TA−TiO_2 NPs show similar morphologies with nanoscale dimensions, because TA is a large polyphenolic compound that

https://dx.doi.org/10.1021/acssuschemeng.0c00860
ACS Sustainable Chem. Eng. 2020, 8, 7359−7370

cannot be polymerized under the experimental conditions used in this study(Figure 2a). The average diameters of TiO_2 and TA−TiO_2 NPs were 25.4 ± 4.89 and 25.1 ± 4.91 nm, respectively [Figure S1, Supporting Information (SI)]. The specific surface areas of TiO_2 and TA−TiO_2 NPs were determined by Brunauer−Emmett−Teller (BET) analysis.[35] The specific surface area of the TA−TiO_2 NPs (58.2 m^2 g^{-1}) was significantly higher than that of the TiO_2 NPs (45.3 m^2 g^{-1}) because of the formation of the porous TA aggregates on the surface of the TiO_2.[15,19] UV−vis spectra show that TA−TiO_2 NPs absorb in the visible region because of LMCT from TA to TiO_2, indicating that excited electrons can be transferred across the interface of the TA−TiO_2 NPs (Figure 2b). According to thermogravimetric analysis (TGA), the residual mass percentages of the TiO_2 and TA−TiO_2 NPs were 97.93% and 92.38%, respectively, which indicates the presence of TA on the TiO_2 surface (Figure 2c). X-ray photoelectron spectroscopy (XPS) and Fourier-transform infrared spectroscopy (FT-IR) analysis (Figure S2) confirmed that the TA layer was well-deposited on the TiO_2 surface. All of these results suggest that the formation of a TA layer on the TiO_2 NPs was successful.

Adsorption Behaviors of Gold Ions onto TA−TiO_2 NPs. To analyze gold adsorption kinetics onto TA−TiO_2 NPs, we measured the gold ion adsorption rates using TiO_2 and TA−TiO_2 NPs in the dark and under AM1.5G solar irradiation at 1-sun intensity [denoted as "(1-sun)"] (Figure 3a). To investigate the gold ion adsorption kinetic profiles on TiO_2 and TA−TiO_2 NPs, we used pseudo-first-order and pseudo-second-order kinetic models,[36,37] where the models assume a linear driving force with one-site and two-site adsorptions, respectively, at the solid/solution interface of an adsorbent. To validate each kinetic model, we determined the correlation coefficient (R^2) values and kinetic parameters by plotting the integral equations [Figure 3c, and Figure S3 and Table S1(SI)]. The results indicate that TiO_2 and TA−TiO_2 NPs followed different kinetics for gold adsorption. For TiO_2 NPs in the dark, most of the gold ions adsorbed onto the TiO_2 NPs within the first hour, with adsorption rates decreasing after 6 h. This result indicates that TiO_2 NPs cannot adsorb and reduce gold ions in the dark. For TiO_2 (1-sun), however, gold adsorption rates increased after 6 h, but they did not fit the pseudo-second-order kinetic model (R^2 = 0.7341) and were much better fitted to the pseudo-first-order kinetic model (R^2 = 0.9911). On the other hand, for TA−TiO_2 NPs, the R^2 values of the pseudo-second-order model (R^2 = 0.9906−0.9952) were much higher than those of the pseudo-first-order model (R^2 = 0.3261−0.9424). This result was supported by fitting theoretical plots of both kinetic models to the experimental results [Figures 3b and S3c (SI)]. The model fitting analysis shows that the TA layer has two adsorption sites that could interact with gold ions, while TiO_2 NPs have just one adsorption site for each gold ion.

The number of metal ions adsorbed onto the adsorbent at equilibrium (q_e, mmol g^{-1}) and the kinetic constant (k_2, g mol^{-1} min^{-1}) were determined using the kinetic parameters of the pseudo-second-order model, and the show the photoenhancement effects of gold adsorption on the TA−TiO_2 NPs (Figure 3c). When compared with the q_e value of TiO_2 (dark) (0.256 mmol g^{-1}), the q_e values for TA−TiO_2 NPs in the dark and TA−TiO_2 NPs (1-sun) were increased by factors of 2.16 (0.522 mmol g^{-1}) and 4.59 (1.175 mmol g^{-1}), respectively. This result demonstrates that the hydroxyl groups in TA are efficient at attracting and adsorbing the gold ions, as demonstrated in our previous work.[24,27] On the other hand, the k_2 values, which indicate the amount of adsorbent required to adsorb 1 mol of metal ions/min, decreased by a factor of 7.0 for TA−TiO_2 (1-sun) (0.08 g $mmol^{-1}$ min^{-1}) in comparison with TA−TiO_2 (dark) (0.56 g $mmol^{-1}$ min^{-1}). This result suggests that light leads to improved adsorption rates of gold ions, probably by reducing the gold ions, which is discussed in the following section.

To further investigate the photoenhancement of gold adsorption, we measured adsorption isotherm curves by incubating 0.5 mg mL^{-1} of TiO_2 and TA−TiO_2 NPs with 0.25, 0.33, 0.5, 1, 1.5, and 2 mM $HAuCl_4$ in the dark and under light irradiation for 3 h at 25 °C (Figure 3d). The number of gold ions adsorbed in the dark by TA−TiO_2 NPs was higher than that adsorbed in the dark by TiO_2 NPs, implying that the presence of TA can increase the adsorption ability of the gold. Moreover, the capacity for gold adsorption increased considerably under light irradiation. To investigate the behavior of gold ion adsorption, we used the Langmuir and Freundlich isotherm models. The Langmuir and Freundlich models describe adsorption at homogeneous and heterogeneous surfaces, indicating the equal and nonequal affinities for adsorbates, respectively.[38] Linearized equations for the Langmuir and Freundlich isotherms are shown in Figures 3e and S4 (SI), respectively. To validate these models, we calculated the R^2 values and isotherm parameters for each isotherm, as summarized in Tables S2 and S3 (SI). For TiO_2 (dark), gold ions were not adsorbed at any concentration; hence, the isotherm models were not fitted for that sample. The experimental adsorption results for TiO_2 (1-sun) and TA−TiO_2 NPs were fitted better to the Langmuir isotherm (R^2 = 0.9578−0.9961) than the Freundlich isotherm (R^2 = 0.8494−0.9775), suggesting that gold ion adsorption at homogeneous sites on the TA layer of TA−TiO_2 NPs can be more properly evaluated using the Langmuir isotherm.

We therefore performed a more thorough evaluation of the adsorption of gold under different illumination conditions using the Langmuir isotherm model. Figure 3f shows the maximum number of gold ions adsorbed on the adsorbents (q_{max}, mmol g^{-1}), as calculated from the inverse of the y-intercept from the Lineweaver−Burk plot. For TiO_2 (dark), K was −34.8640 L $mmol^{-1}$ and q_{max} was 0.0968 mmol g^{-1}. On the other hand, TA−TiO_2 (dark) exhibited K = 5.7382 L $mmol^{-1}$ and q_{max} = 0.7909 mmol g^{-1}, which correspond to about −0.16 and 8.2 times the values obtained for TiO_2 (dark), respectively. These results indicate that the TA coating effectively improved gold ion adsorption onto the surface, most definitely by Au ion−galloyl complexation.[39] Moreover, the light illumination improved this adsorption significantly. The adsorption isotherm of gold ions on TiO_2 (1-sun) also showed Langmuir-type adsorption with K = 0.4542 L $mmol^{-1}$ and q_{max} = 2.4755 mmol g^{-1}, which correspond to about −0.01 and 25 times the values obtained for these using TiO_2 (dark), respectively. These results indicate that the illumination of TiO_2 NPs with light can increase the adsorption of gold ions. The isotherm for gold adsorption on TA−TiO_2 (1 sun) also exhibited Langmuir-type adsorption, with K = 0.2416 L $mmol^{-1}$ and q_{max} = 8.8365 mmol g^{-1}, corresponding to approximately 0.04 and 11.17 times the values obtained for TA−TiO_2 (dark), respectively. The K value was much smaller than that of TA−TiO_2 (dark), and the q_{max} value was significantly increased, which can be the result of prolonged

https://dx.doi.org/10.1021/acssuschemeng.0c00860
ACS Sustainable Chem. Eng. 2020, 8, 7359−7370

electron lifetime due to direct Z-scheme behavior from the combination of TA and TiO_2, as well as surface plasmon resonance by the AuNPs formed from the reduced gold ions. The q_{max} and photoenhanced factor of TA−TiO_2 NPs were 5.3 and 1.9 times higher, respectively, than those of the TA-coated polymer microspheres (1.635 mmol g^{-1} and 5.9 times).[27] Table 1 indicates that the TA−TiO_2 NPs with 1-sun irradiation exhibit the highest maximum gold ion adsorption capacity among the absorbents reported in the literature. The result suggests that the photochemical enhancement using the direct Z-scheme heterostructure with polyphenol chemistry has considerable potential for gold ion recovery from E-waste and industrial wastewater. Moreover, the result indicates that the direct Z-scheme heterojunction is an effective means of overcoming the drawbacks of a single-component photochemical reaction.

Table 1. Comparison of Gold Adsorption Capacities of TA−TiO_2 NPs and Conventional Adsorbents Reported in the Literature

adsorbents	maximum gold adsorption capacity		ref
	mmol/g	mg/g	
TA-coated TiO_2 NPs with 1-sun irradiation	8.84	1741.1	this work
TA-coated microspheres with 1-sun irradiation	1.64	323.0	27
thiol- and amine-functionalized rice straw	2.28	449.1	10
functionalized activated carbon	0.16	32.3	40
activated carbon modified with 2,6-diaminopyridine	1.03	202.7	41
oxidized multiwalled carbon nanotubes	0.32	62.3	42
amidoxime-functionalized polymer microspheres	2.32	456.7	7
amine-functionalized mesoporous silica	1.4	275	8

Images from transmission electron microscopy (TEM) (Figure 4) and scanning electron microscopy with a backscattered electron detector (BSE-SEM) (Figure S7, SI) show that the number of AuNPs adsorbed on TA−TiO_2 NPs (1-sun) was much higher than that on TA−TiO_2 NPs (dark). For TiO_2 NPs (1-sun), AuNPs were much larger than TiO_2NPs,

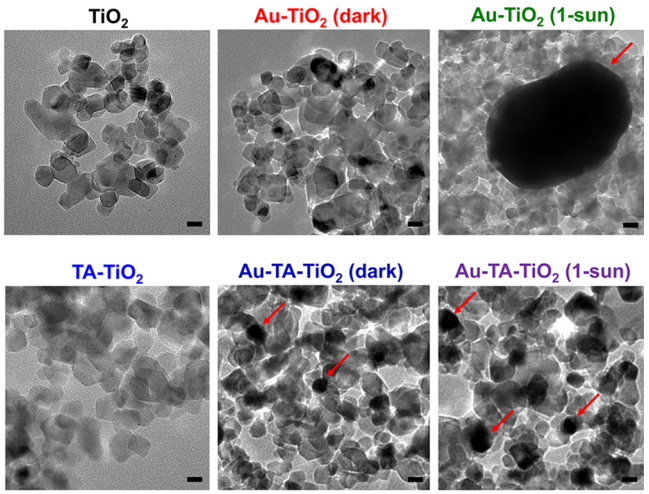

Figure 4. TEM images of TiO_2, Au−TiO_2, TA−TiO_2, and Au−TA−TiO_2 (scale bar: 20 nm).

indicating that AuNPs were not adsorbed on the TiO_2 surface. X-ray diffraction (XRD) analysis of TiO_2 and TA−TiO_2 before and after gold adsorption was used to confirm the reduction of gold ions (Figure 5a). Before gold adsorption, the XRD spectra of TiO_2 and TA−TiO_2 exhibited same peaks for the anatase (2θ = 25.31°, 37.85°, 48.05°, 55.08°, 62.74°, and 75.11°) and rutile phases (2θ = 27.45°, 36.09°, 41.23°, 54.32°, 69.01°, and 69.79°). After gold adsorption, the XRD spectra of Au−TiO_2 and Au−TA−TiO_2 exhibited four additional peaks at 2θ = 38.19°, 44.38°, 64.49°, and 77.47°, which correspond to the (111), (200), (220), and (311) planes of the face-centered cubic lattice of gold, respectively. The intensity of the gold peaks was related to the gold adsorption rates. To better understand the photochemical activity of TA−TiO_2 NPs, we obtained light absorption spectra for TiO_2, TA−TiO_2, and Au−TA−TiO_2 NPs (Figure 5b). UV−vis spectra showed that absorbance in the visible region (400−600 nm) was significantly increased by the TA coating. TA−TiO_2 showed broad absorption in the UV- and visible-light ranges due to metal-to-ligand charge transfer (MLCT) between TA and TiO_2 as well as electronic transitions within TA (e.g., $\pi-\pi$ conjugation and hydrogen bonding), while this was not seen for the untreated TiO_2 NPs. Au−TA−TiO_2 NPs showed a broad absorption peak around 400−800 nm because of LSPR generated by the AuNPs, which adsorbed on the TA layer. This result indicates that the gold ions were reduced to metallic gold by the TA layer. The surface properties of TiO_2 NPs and TA−TiO_2 NPs after gold adsorption were also investigated by XPS (Figure 5c). For both nanoparticles, significant Au^0 4f peaks were observed at 87.7 and 84.0 eV, with small Au^{1+} and Au^{3+} peaks due to Au ion−catechol complexes.[27,39] However, the percentage of Au^{3+} 4f peaks in TA−TiO_2 (1-sun) was much lower than seen for TA−TiO_2 (dark) (Figure 5d). For TA−TiO_2 NPs, the atomic percentage of metallic gold (Au^0) increased under light illumination. These results indicate that most gold ions were reduced to metallic gold on the TA layer, particularly under light illumination.

Light-Induced Enhancement of Gold Adsorption by TA−TiO_2. We propose a direct Z-scheme mechanism for photochemically increased gold ion adsorption when irradiating TA−TiO_2 NPs, as illustrated in Figure 6. The energy level and band gap of TiO_2 and TA−TiO_2 NPs were determined using ultraviolet photoelectron spectroscopy (UPS) and reflection electron energy loss spectroscopy (REELS), respectively. (Figure S5, SI). In the dark, by two successive proton-coupled electron transfers (PCET), the phenolic group is oxidized to quinone,[27,43−45] whereas gold ions are reduced due to the different redox potentials of TA and gold ions. TiO_2 has no ability to reduce gold ions in the dark; however, under light irradiation, a synergetic photocatalytic effect takes place via a direct Z-scheme from TiO_2 to TA. TA has a highest occupied molecular orbital (HOMO) level and a lowest unoccupied molecular orbital (LUMO) level, while TiO_2 has a valence band (VB) and a conduction band (CB). Both TA and TiO_2 are excited under light illumination, leading to excitation of electrons from the HOMO of TA and the VB of TiO_2 to the LUMO of TA and the CB of TiO_2, respectively, leaving holes in the HOMO of TA and the VB of TiO_2. Notably, the difference between the energy bands of TiO_2 and TA allows the recombination of the electrons in the CB of TiO_2 and the holes in the HOMO of TA. These characteristics allow the interface to serve as an internal electric field for the pathway of

https://dx.doi.org/10.1021/acssuschemeng.0c00860
ACS Sustainable Chem. Eng. 2020, 8, 7359−7370

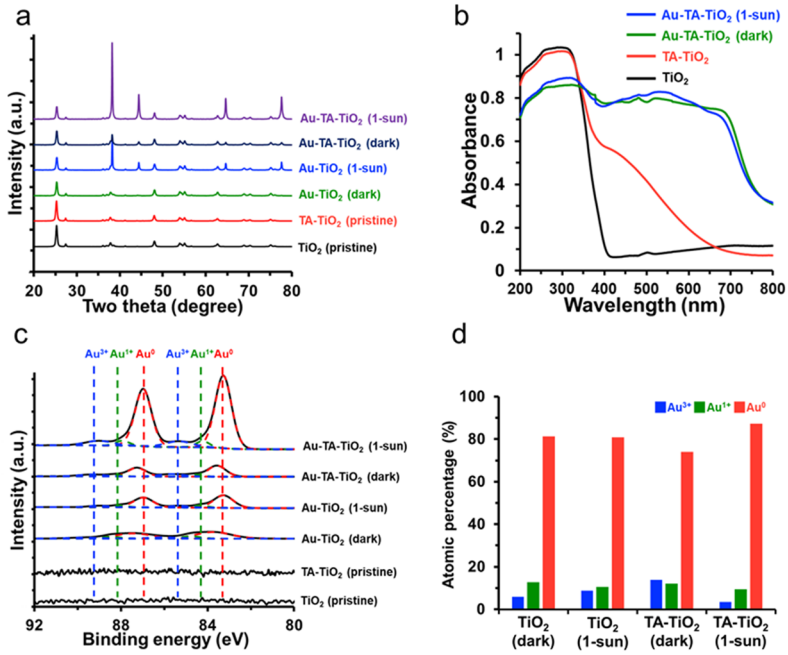

Figure 5. (a) XRD patterns of TiO_2 NPs and TA−TiO_2 NPs before and after gold adsorption. (b) UV−vis absorption spectra of TiO_2 NPs (black), TA−TiO_2 NPs (red), Au−TA−TiO_2 NPs, dark (green), and Au−TA−TiO_2 NPs (1-sun) (blue). (c) XP spectra for Au 4f of TiO_2 and TA−TiO_2 NPs after gold adsorption using 2 mM $HAuCl_4$ in the dark and under light irradiation. (d) Atomic percentage of Au species obtained through the Au species peak region from the XP spectra.

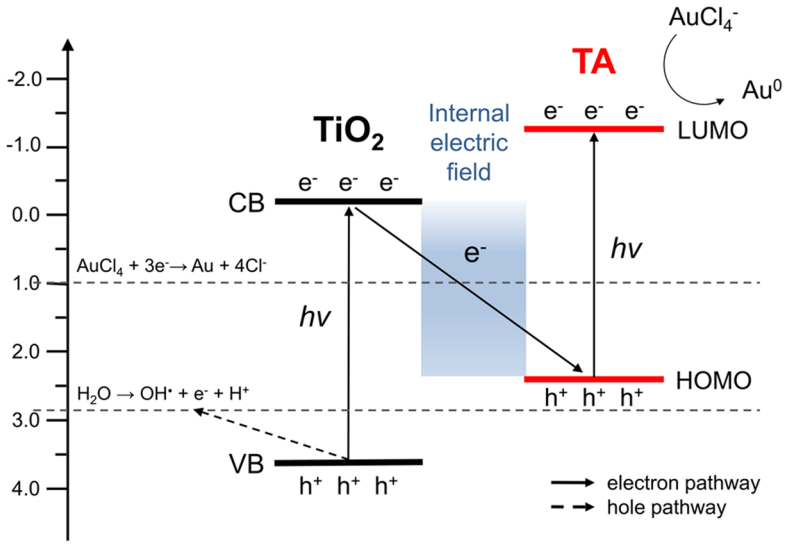

Figure 6. Schematic diagram of the photochemical mechanism of gold adsorption using TA−TiO_2 NPs.

electron transfer. Therefore, photoexcited electrons in the CB of TiO_2 transfer through the interface to the HOMO of TA and then recombine with the electron−hole pairs, thereby extending the lifetime of photoexcited electrons in the LUMO of TA. Then, the electrons in the LUMO of TA participate in the gold adsorption cycle. On the other hand, the photogenerated holes on the surface of TiO_2 must be consumed due to the retarded electron−hole pair recombination in TiO_2, which occurs due to continuous electron transfer by the direct Z-scheme mechanism. The holes can move quickly and are consumed by the oxidation of water molecules, and the generated hydroxyl radicals are scavenged by TA. This mechanism can facilitate the process of charge separation and thus improve the photocatalytic activity, leading to exceptionally high gold adsorption efficiencies.

To verify the proposed mechanism, we measured the lifetimes of the excited electrons using a fluorescence lifetime spectrometer (FLS), as shown in Figure 7a. The lifetime in TA−TiO_2 (362.1 ns) was about 2.2 times longer than in TiO_2 (163.4 ns). The prolonged carrier lifetime in TA−TiO_2 NPs represents efficient charge transfer between TA and TiO_2, followed by direct Z-scheme heterojunction behavior, which can retard recombination of electron−hole pairs in TA.[46,47] The behavior of charge transfer was also investigated using photocurrent measurements (Figure 7b) in a three-electrode system, where TiO_2/indium−tin oxide (ITO) electrodes

https://dx.doi.org/10.1021/acssuschemeng.0c00860
ACS Sustainable Chem. Eng. 2020, 8, 7359−7370

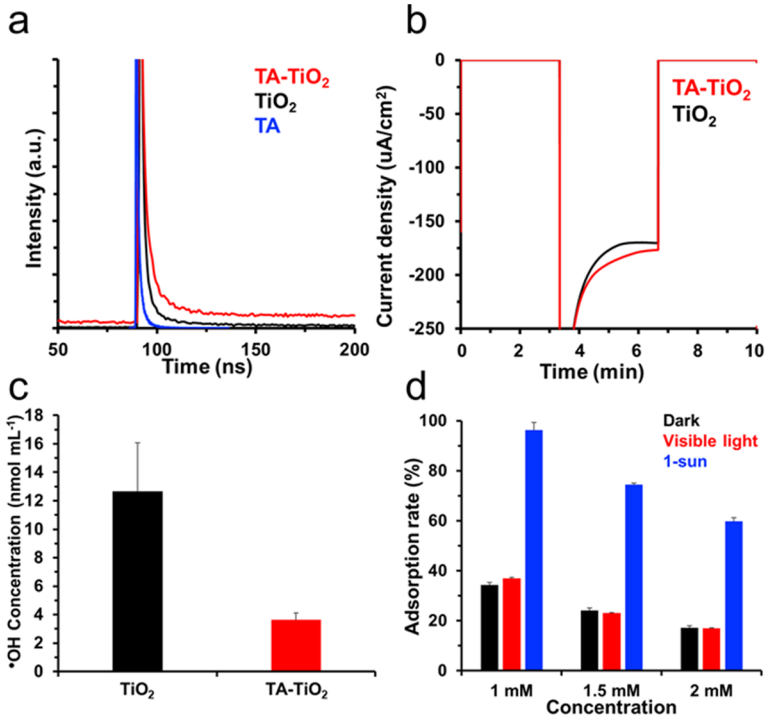

Figure 7. (a) Fluorescence lifetime measurements of TA, TiO_2 NPs, and TA−TiO_2 NPs. (b) Photocurrents of TiO_2 and TA−TiO_2 NPs at an applied potential of 0.4 V vs the normal hydrogen electrode (NHE) under 1-sun illumination. (c) Concentrations of hydroxyl radicals generated by TiO_2 and TA−TiO_2 NPs under 1-sun illumination for 5 min. (d) Gold adsorption rates at different gold ion concentrations.

coated with TA were used as photoanodes. The cathodic bias used for the photocurrent measurements represents electron transfer from the TiO_2 to TA. In accordance with the increase in gold adsorption activity, the photocurrents obtained using TA−TiO_2 electrodes were higher than those using TiO_2 electrodes. This result indicates that TA can efficiently absorb light and that excited electrons can be transferred through the interface of the TA−TiO_2 NPs.

On the other hand, the holes generated in the VB of TiO_2 should be consumed, to prevent undesirable backward reactions and the recombination of electron−hole pairs in TiO_2 and to allow electron transfer via the direct Z-scheme pathway. Holes generated in TiO_2 are known water oxidants;[30] therefore, the amount of holes generated on the surface of TiO_2 can be estimated by the number of hydroxyl radicals in the solution. Therefore, we measured the concentration of hydroxyl radicals generated by TiO_2 and TA−TiO_2 NPs after UV illumination for 5 min (Figure 7c) and found that hydroxyl radicals were suppressed due to the presence of TA. This result shows that the holes in the VB of TiO_2 can be consumed by TA.[32]

To verify the pathway of the excited electrons, we examined the gold adsorption behavior under visible-light illumination (Figure 7d). The gold ion adsorption rate of TA−TiO_2 NPs was similar in the dark and under visible-light irradiation, regardless of the concentration of gold ions. Since visible-light illumination had no significant effect, it can be inferred that excited electrons generated via LMCT cannot affect the gold adsorption efficiency, meaning that only electrons in the LUMO level of TA can be involved in the reduction of gold ions. To verify the conversion of catechol to quinone due to the adsorption of gold ions, we obtained XP spectra for O 1s of TA−TiO_2, Au−TA−TiO_2 (dark), and Au−TA−TiO_2 (1-sun) (Figure S6, SI). The atomic percentage of O species (Figure S6b, SI) shows that catechol in TA converted to quinone after the gold ions were adsorbed. The amount of adsorbed gold ions and quinone in Au−TA−TiO_2 (1-sun) was considerably higher than that in Au−TA−TiO_2 (dark), supporting that the adsorption of gold ions induced the conversion of catechol to quinone. All of the above results suggest that the enhanced gold ion adsorption activity of TA−TiO_2 NPs under 1-sun irradiation can be explained by the direct Z-scheme mechanism. We expect that other adhesive polyphenolic compounds can be applied for gold ion recovery through the same mechanism proposed in this work.

Metal Selectivity of TA−TiO_2 under Light Irradiation. High selectivity toward the target metal ions is essential because industrial wastewater contains various precious metals (e.g., gold, palladium, and platinum) and base metals (e.g., iron, nickel, copper, cobalt, zinc, and aluminum).[48] To demonstrate the selectivity of TA−TiO_2 NPs toward gold ions, we performed adsorption experiments using a mixture of various metal chlorides, gold, platinum, copper, cobalt, nickel, zinc, iron, palladium, and aluminum, which are known to be the main components of electronic waste.[48,49] TiO_2 and TA−TiO_2 NPs were immersed in 1 mM metal ion mixtures for 3 h, and the adsorption rates of the metal species on the TA−TiO_2 NPs were calculated by the concentration of metal ions in the supernatant, measured by ICP-OES (Figure 8). TiO_2 NPs in the dark showed no adsorption ability toward gold ions, while iron ions exhibited significant adsorption (~40%). TiO_2 (1-sun) and TA−TiO_2 in the dark exhibited gold adsorption capability, but iron ions were also adsorbed on the samples. Iron ions are known ionic dopants for TiO_2 due to their similar ionic radii (Fe^{3+}, 0.69 Å; Ti^{4+}, 0.75 Å). Under 1-sun simulated light, however, the TA−TiO_2 NPs exhibited high adsorption capability (>99%) and high selectivity toward gold ions, while no other metal ions showed significant adsorption, indicating

https://dx.doi.org/10.1021/acssuschemeng.0c00860
ACS Sustainable Chem. Eng. 2020, 8, 7359−7370

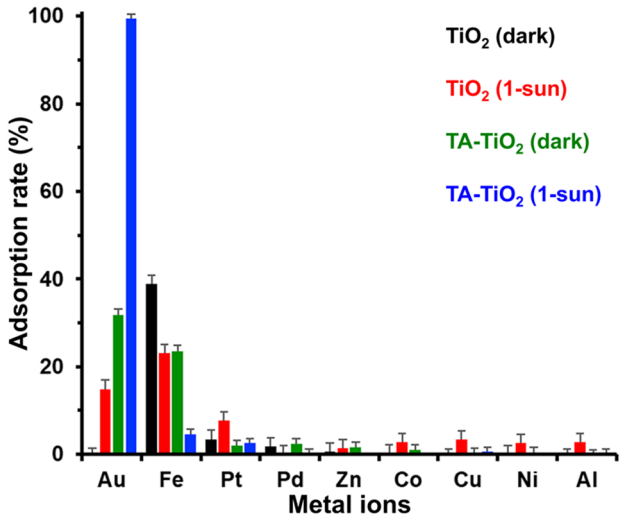

Figure 8. Adsorption selectivity toward gold ions among 1 mM of nine different metal chloride ions (Au, Fe, Pt, Pd, Zn, Co, Cu, Ni, and Al) using TiO_2 NPs in the dark (black), TiO_2 NPs under 1-sun illumination (red), TA−TiO_2 NPs in the dark (green), and TA−TiO_2 NPs under 1-sun illumination (blue).

that only the excited electrons of TA can participate in the adsorption process.

Au^{3+} has a higher reduction potential than other precious metals and base metals (E^0 = 1.002 V for $AuCl_4^-$, E^0 = 0.76 V for $PtCl_4^{2-}$, E^0 = 0.68 V for $PtCl_6^{2-}$, and E^0 < 0.6 V for base metals).[50,51] This higher redox potential contributes to the selective adsorption of gold from the solution. It is known that platinum chloride is relatively inert when compared to gold chloride, resulting in a low binding efficiency to TA−TiO_2 NPs, despite the high redox potential of platinum.[52] TA and polyphenolic groups chelate base metal ions (e.g., iron, copper, nickel, and zinc); however, they form reversible complexes with polyphenolic compounds under acidic conditions, which are not suitable for the selective adsorption of base metal ions.[44,53,54] By contrast, gold ions were not detected in the supernatant after the treatment, indicating stable adsorption to TA.

The results suggest that the TA layer has an extremely high selectivity for gold ions, especially under light irradiation, with other metal species hardly affecting the gold ion adsorption. The different reduction energies originate from their inherent redox potentials; for instance, zinc and aluminum have very low redox potentials, while iron has a moderate redox potential. Therefore, we believe that this approach can be extended for the selective recovery of other metal ions by tuning the redox potential of TA or using other polyphenolic materials.

Gold Desorption from Au-Adsorbed TA−TiO_2 NPs. Next, we investigated the recovery of metallic gold from Au−TA−TiO_2 NPs through desorption by acid treatment using a mixture of hydrochloric acid and nitric acid. TiO_2 NPs were stable during the acid treatment using dilute aqua regia; however, gold nanoparticles were desorbed and dissolved after the desorption process. Although Au NPs were observed in the BSE-SEM image of Au−TA−TiO_2 before the desorption process (represented as white spots in Figure 9a), most Au NPs were removed by treatment with an acidic solution at 25 °C for 3 h (Figure 9b). To further investigate the desorption of gold from nanoparticles, we performed XPS and XRD analyses of Au−TA−TiO_2. In the XP spectra, Au 4f peaks for Au^0, Au^{1+}, and Au^{3+} were found before desorption, whereas no Au 4f peaks existed after desorption (Figure 9c). Before the

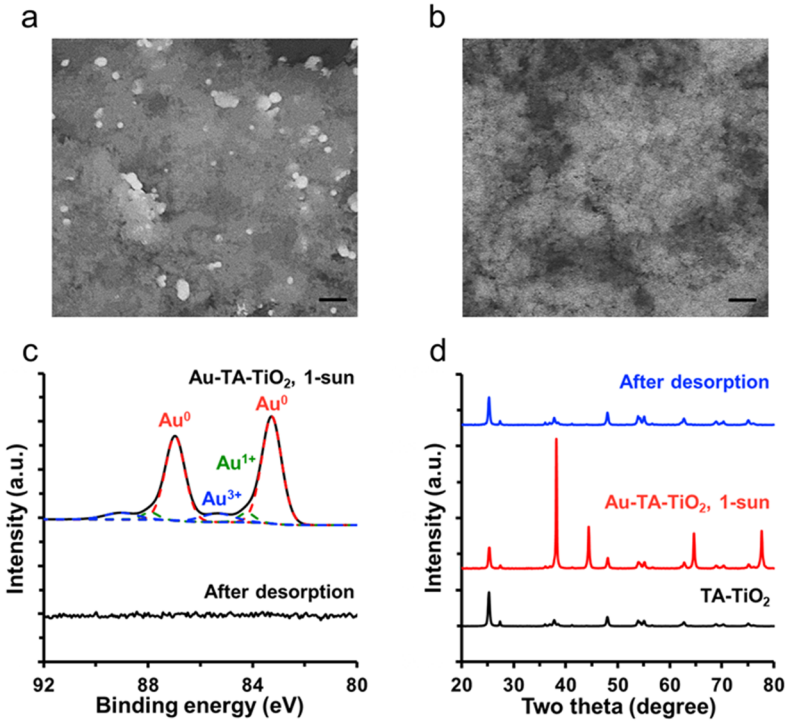

Figure 9. BSE-SEM images of Au−TA−TiO_2 NPs before (a) and after (b) desorption. (c) XP spectra for Au 4f of Au−TA−TiO_2 NPs before and after desorption and (d) XRD patterns of Au−TA−TiO_2 NPs before and after desorption.

https://dx.doi.org/10.1021/acssuschemeng.0c00860
ACS Sustainable Chem. Eng. 2020, 8, 7359−7370

desorption process, four peaks were observed in the XRD analysis at 2θ = 38.14°, 44.28°, 64.5°, and 77.52°, corresponding to the (111), (200), (220), and (311) planes of metallic gold, respectively. However, these peaks disappeared after desorption (Figure 9d). Moreover, the amounts of gold on the Au−TA−TiO_2 NPs before and after the desorption process were measured by ICP-OES. The amount of gold ions in Au−TA−TiO_2 NPs before and after desorption was 23 545 and 131.4 mg kg^{-1}, respectively, corresponding to 99.4% recovery, while that of gold ions collected using TiO_2 (dark), TiO_2 (1-sun), and TA−TiO_2 (dark) was 85.3, 10 795, and 6842 mg kg^{-1}, respectively. These results indicate that TA−TiO_2 NPs under light illumination possess significantly higher gold ion recovery compared to others. These results indicate that acid treatment can efficiently dissociate adsorbed gold from the TA layer. Although the TA layer decomposed after desorption, TiO_2 NPs can be reused by additional TA coatings for gold ion recovery. After readsorption on TA−TiO_2 NPs, the amount of gold ions in Au−TA−TiO_2 NPs was 23 337 mg kg^{-1}, indicating that the reused particles can successfully facilitate gold ion recovery.

CONCLUSIONS

This study demonstrated that polyphenol-coated semiconductor materials can significantly increase the adsorption efficiency for gold ions under light illumination through a direct Z-scheme mechanism. The TA−TiO_2 NPs were prepared by a dipping method. Under simulated 1-sun light illumination, both TA and TiO_2 generated excited electrons and holes. MLCT from TA and TiO_2 extended the lifetime of the excited electron on TA, resulting in the recombination of the electrons of TiO_2 and the holes of TA. The excited electrons with prolonged lifetimes on the TA layer then allowed for the efficient gold ion adsorption from the solution. Additionally, the presence of TA significantly scavenges the ROS created by the holes generated within the TiO_2 surface, indicating that there is no need for hole scavengers in the photochemical reaction. These combined effects led to enhanced gold adsorption capacity, and this was seen in that the maximum amount of adsorbed gold ions was increased by a factor of 11 under 1 sun of simulated light compared to in the dark. The adsorbed gold on the TA−TiO_2 NPs could be simply removed using acidic solutions. High selectivity toward gold ions from mixtures of metal ion was also demonstrated, indicating that the TA−TiO_2 heterostructures can adsorb and reduce gold ions with high capacity and selectivity. We expect that mimicking the natural photosynthetic Z-scheme system using bioinspired polyphenol chemistry and semiconductor materials can provide low-cost, ecofriendly adsorbents for metal ion recovery with high capacity and selectivity.

EXPERIMENTAL METHODS

Materials. Titanium dioxide (TiO_2) nanoparticles (Degussa P25), tannic acid (TA), gold(III) chloride trihydrate ($HAuCl_4{\cdot}3H_2O$, 99.9%), platinum(IV) chloride hexahydrate ($H_2PtCl_6{\cdot}6H_2O$, 99.9%), copper(II) chloride dihydrate ($CuCl_2{\cdot}2H_2O$, 99%), cobalt(II) chloride hexahydrate ($CoCl_2{\cdot}6H_2O$, 98%), nickel(II) chloride hexahydrate ($NiCl_2{\cdot}6H_2O$, 99.9%), zinc chloride ($ZnCl_2$, 98%), iron(III) chloride hexahydrate ($FeCl_3{\cdot}6H_2O$, 98%), aluminum chloride hexahydrate ($AlCl_3{\cdot}6H_2O$, 99%), palladium(II) chloride ($PdCl_2$, 99%), and terephthalic acid (TAc) were purchased from Sigma-Aldrich (St. Louis, MO). Sodium hydroxide was obtained from Junsei Chemical (Tokyo, Japan). Ethanol (94.5%) was purchased from Daejung Chemicals (Siheung, Republic of Korea). Milli-Q water was used as deionized water in all experiments. Hydroxyterephthalic acid (2-HTAc) was obtained from Tokyo Chemical Industry (Tokyo, Japan).

Synthesis of TA−TiO_2 NPs. TiO_2 NPs (300 mg) were dispersed in 27 mL of deionized water, and 3 mL of TA solution (10 mg mL^{-1}) was added into the TiO_2 dispersion. The mixture was magnetically stirred at 300 rpm and 25 °C for 1 h. The TA−TiO_2 NPs were collected by centrifugation at 7000g for 5 min and rinsed two times with 35 mL of a 2:1 (v/v) mixture of ethanol and Milli-Q water. The treated TA−TiO_2 NPs were dried in a vacuum oven for 1 h before further investigation. The structural morphologies and characteristics of the nanoparticles were analyzed by TGA, FT-IR, SEM, and BET methods.

Light-Induced Gold Adsorption Kinetics. Gold ion precursors were prepared by dissolving $HAuCl_4$ in Milli-Q water at a concentration of 1 mM. The TiO_2 NPs and TA−TiO_2 NPs were added to 5 mL of 1 mM $HAuCl_4$ solution at a concentration of 0.5 mg mL^{-1} and then exposed to light (AM1.5G solar illumination at 1-sun intensity) at room temperature. After adsorption times of 5, 15, 30, and 60 min, 1 mL of the supernatant was extracted. The nanoparticles were collected by centrifugation at 7000g for 5 min, and the supernatants were diluted with deionized water to measure the remaining concentration of gold ions using ICP-OES. As a control experiment, adsorption was also performed in the dark using the same procedure. The number of adsorbed gold ions at time t (q_t, mmol g^{-1}) was calculated using the following equation: $q_t = \frac{C_i - C_t}{W} \times V$, where C_i and C_t (mM) = the concentrations of gold ions at the initial time and time t, respectively, W (g) = the weight of the adsorbent, and V (L) = the volume of the solution. The adsorption kinetics was analyzed using a pseudo-first-order kinetics model, $\frac{dq_t}{dt} = k_1(q_e - q_t)$, and a pseudo-second-order kinetics model, $\frac{dq_t}{dt} = k_2(q_e - q_t)^2$, where q_e and q_t = the number of adsorbed gold ions at equilibrium time and time t, respectively, k_1 = the pseudo-first-order rate constant, and k_2 = the pseudo-second-order rate constant.[36,37]

Light-Induced Adsorption of Gold Ion Precursors. Gold ion precursors were prepared by dissolving $HAuCl_4$ in Milli-Q water at concentrations of 0.25−2 mM. The TiO_2 NPs and TA−TiO_2 NPs were added to 3 mL of $HAuCl_4$ solution at a concentration of 0.5 mg mL^{-1} and were then exposed to light at 25 °C either in the dark or under light illumination. The nanoparticles were collected by centrifugation at 7000g for 5 min, and the supernatants were collected to measure the remaining concentration of gold ions by ICP-OES. The adsorption isotherm was analyzed using the Lineweaver−Burk equation for the Langmuir isotherm curves, $q^{-1} = q_{max}^{-1} + (q_{max}KC)^{-1}$, and the linearized Freundlich isotherm curves, $\log q = \log K_F + \frac{1}{n}\log C$, where q = the number of gold ions adsorbed on the adsorbents, q_{max} = the maximum amount of gold ions adsorbed on the adsorbents, K = the Langmuir equilibrium constant, K_F = the Freundlich isotherm constant, n = the constant for adsorption intensity, and C = the bulk concentration of gold ions.

Photoelectrochemical Analysis of TA−TiO_2 NPs. To measure the photocurrents of the TiO_2 and TA−TiO_2 nanoparticles, TiO_2 films on 1.5 × 1 cm ITO glass slides were prepared in accordance with previous reports.[33] In brief, TiO_2 NPs were ground with a pestle in a mortar with deionized water (1 mL) containing acetylacetone (100 μL). Additional deionized water (1.7 mL) was slowly added to the paste with continuous grinding. One drop of Triton-X100 was added to the paste and grinding continued until a homogeneous TiO_2 paste was obtained. Approximately 2 mm of the edge of an ITO glass slide was covered with Scotch tape (thickness ~62.5 μm). The TiO_2 paste (100 μL) was place on the substrate and spread using a razor blade. The TiO_2 paste spread on the glass slide was then dried at 70 °C for 10 min, followed by incubation in a furnace at 400 °C for 45 min. The TiO_2 films were then immersed in TA solution (10 mg mL^{-1}) for 1 h at room temperature. The pristine and TA-coated TiO_2 films were used for photoelectrochemical analysis.

https://dx.doi.org/10.1021/acssuschemeng.0c00860
ACS Sustainable Chem. Eng. 2020, 8, 7359−7370

Hydroxyl Radical Analysis. TAc was used to ascertain the concentration of hydroxyl radicals that are formed by the oxidation of water by TiO_2. TAc solution was prepared by dissolving TAc in 4 mM NaOH at a concentration of 1 mM. The TiO_2 NPs and TA−TiO_2 NPs were added to 1 mL of 0.5 mM TAc solution at a concentration of 0.05 mg mL^{-1} and then exposed to light (1-sun) at 25 °C for 5 min. After exposure, the mixtures were centrifuged at 7000*g* for 5 min to extract the supernatant, and the concentrations of residual hydroxyl radicals in each sample were then determined by fluorescence spectroscopy. Pure 2-HTAc was used to generate a calibration curve for the hydroxyl radicals.

Gold Desorption from Au-Adsorbed TiO_2 Nanoparticles. Desorption experiments were performed on Au-adsorbed nanoparticles using acidic solutions. Au−TA−TiO_2 NPs were prepared using the procedures described above, with 2 mM solutions of $HAuCl_4$ under AM1.5G solar illumination at 1-sun intensity. Acidic solutions were prepared by mixing 0.7 M HCl and 0.3 M HNO_3 solutions. The Au−TA−TiO_2 NPs were added to 10 mL of the acidic solution and then magnetically stirred for 3 h at 300 rpm and 25 °C. The nanoparticles were centrifuged and washed at 7000*g* for 5 min. The amounts of gold on the nanoparticles and in the supernatant were analyzed by BSE-SEM, XPS, XRD, and ICP-OES to calculate the percentage of gold desorbed from the prepared nanoparticles.

Metal Selectivity of the TA−TiO_2 NPs. A mixed metal chloride solution was used to investigate the metal selectivity of the TA−TiO_2 NPs. Nine metal chloride ions (Au, Pt, Cu, Co, Ni, Zn, Fe, Pd, and Al) at a concentration of 1 mM were used, representing the primary components of electronic waste.[49,55] The TiO_2 NPs and TA−TiO_2 NPs were immersed in 3 mL of this solution at a concentration of 0.5 mg mL^{-1} and then exposed to light for 3 h at 25 °C. The nanoparticles were then collected by centrifugation at 7000*g* for 5 min. The supernatants were used to measure the remaining concentrations of the metal ions using ICP-OES.

Characterization. The morphologies of the nanoparticles were examined using SEM (Hitachi SU5000, Hitachi, Ltd., Tokyo, Japan) at an acceleration voltage of 10 kV. The elemental compositions were analyzed using XPS (Thermo Scientific Sigma Probe, Thermo Fisher Scientific, Inc., Waltham, MA). XRD patterns of the TiO_2 NPs and Au-adsorbed TiO_2 NPs were obtained using a powder X-ray diffractometer (Rigaku D/MAX-2500, Rigaku, Tokyo, Japan). The functional groups of the nanoparticles were analyzed using FT-IR (JASCO, Easton, MD). A xenon lamp (HAL-320 Solar Simulator, Asahi Spectra Co., Ltd., Tokyo, Japan) was used as the light source. The amounts of metal ions were quantitatively analyzed using ICP-OES (Agilent ICP-OES 5110, Agilent, Santa Clara, CA). The surface areas of the nanoparticles were determined by BET analysis (3-Flex, Micromeritics, Norcross, GA). The energy levels and band gap of TiO_2 and TA−TiO_2 NPs were determined using UPS (Sigma Probe, Thermo VG Scientific, Waltham, MA) and REELS (Axis-Supra, Kratos, Duisburg, Germany), respectively. Electron decay times of TA, TiO_2, and TA−TiO_2 NPs were measured using FLS (FL920, Edinburgh Instruments, Livingston, Scotland). Photocurrent and CV measurements were carried out using a conventional three-electrode system connected to a computer-controlled potentiostat (Ivium, Eindhoven, Netherlands). The photoelectrochemical (PEC) cell contained a photoanode, a coiled Pt wire, and Ag/AgCl (saturated KCl) electrode as the working, counter, and reference electrodes, respectively. The concentrations of residual hydroxyl radicals were analyzed using a microplate reader (CLARIO star, BMG Labtech, Ortenberg, Germany) at an excitation wavelength of 320 nm and emission wavelengths of 350−600 nm.

■ ASSOCIATED CONTENT

Supporting Information

The Supporting Information is available free of charge at https://pubs.acs.org/doi/10.1021/acssuschemeng.0c00860.

Particle size distribution of TiO_2 and TA−TiO_2 NPs, XP spectra for C 1s, FT-IR spectra of TiO_2 and TA−TiO_2 NPs, adsorption kinetic models of TiO_2 and TA−TiO_2 NPs, correlation coefficients and kinetic parameters obtained from adsorption kinetic models and isotherm models, and BSE-SEM images of TiO_2, Au−TiO_2, TA−TiO_2, and Au−TA−TiO_2 NPs (PDF)

■ AUTHOR INFORMATION

Corresponding Author

Yoon Sung Nam − *Department of Materials Science and Engineering and KAIST Institute for Nanocentury, Korea Advanced Institute of Science and Technology, Daejeon 34141, Republic of Korea;* orcid.org/0000-0002-7302-6928; Email: yoonsung@kaist.ac.kr

Authors

Kyeong Rak Kim − *Department of Materials Science and Engineering, Korea Advanced Institute of Science and Technology, Daejeon 34141, Republic of Korea;* orcid.org/0000-0001-8007-6272

Saehan Choi − *Department of Materials Science and Engineering, Korea Advanced Institute of Science and Technology, Daejeon 34141, Republic of Korea;* orcid.org/0000-0002-0449-4621

Cafer T. Yavuz − *Graduate School of Energy, Environment, Water and Sustainability, Department of Chemical and Biomolecular Engineering, and Department of Chemistry, Korea Advanced Institute of Science and Technology, Daejeon 34141, Republic of Korea;* orcid.org/0000-0003-0580-3331

Complete contact information is available at: https://pubs.acs.org/10.1021/acssuschemeng.0c00860

Notes

The authors declare no competing financial interest.

■ ACKNOWLEDGMENTS

This research was supported by CTK Cosmetics (Republic of Korea) and the Nano-Material Technology Development Program through the National Research Foundation of Korea (NRF), funded by the Ministry of Science, ICT, and Future Planning (NRF-2017M3A7B4042235 and NRF-2017M3A7B4052797).

■ REFERENCES

(1) Isıldar, A.; Rene, E. R.; van Hullebusch, E. D.; Lens, P. N. L. Electronic Waste as a Secondary Source of Critical Metals: Management and Recovery Technologies. *Resour. Conserv. Recycl.* **2018**, *135*, 296−312.

(2) Zhang, L.; Xu, Z. A Review of Current Progress of Recycling Technologies for Metals from Waste Electrical and Electronic Equipment. *J. Cleaner Prod.* **2016**, *127*, 19−36.

(3) Bukasov, R.; Shumaker-Parry, J. S. Highly Tunable Infrared Extinction Properties of Gold Nanocrescents. *Nano Lett.* **2007**, *7* (5), 1113−1118.

(4) Rao, M. D.; Singh, K. K.; Morrison, C. A.; Love, J. B. Challenges and Opportunities in the Recovery of Gold from Electronic Waste. *RSC Adv.* **2020**, *10* (8), 4300−4309.

(5) De Gisi, S.; Lofrano, G.; Grassi, M.; Notarnicola, M. Characteristics and Adsorption Capacities of Low-Cost Sorbents for Wastewater Treatment: A Review. *Sustain. Mater. Technol.* **2016**, *9*, 10−40.

(6) Dong, Z.; Liu, J.; Yuan, W.; Yi, Y.; Zhao, L. Recovery of Au(III) by Radiation Synthesized Aminomethyl Pyridine Functionalized Adsorbents Based on Cellulose. *Chem. Eng. J.* **2016**, *283*, 504−513.

(7) Dogan, N. A.; Hong, Y.; Ozdemir, E.; Yavuz, C. T. Nanoporous Polymer Microspheres with Nitrile and Amidoxime Functionalities for

Gas Capture and Precious Metal Recovery from E-Waste. *ACS Sustainable Chem. Eng.* **2019**, *7*, 123−128.
(8) Lam, K. F.; Fong, C. M.; Yeung, K. L.; Mckay, G. Selective Adsorption of Gold from Complex Mixtures Using Mesoporous Adsorbents. *Chem. Eng. J.* **2008**, *145*, 185−195.
(9) Won, S. W.; Kotte, P.; Wei, W.; Lim, A.; Yun, Y. S. Biosorbents for Recovery of Precious Metals. *Bioresour. Technol.* **2014**, *160*, 203−212.
(10) Wang, J.; Li, J.; Wei, J. Adsorption Characteristics of Noble Metal Ions onto Modified Straw Bearing Amine and Thiol Groups. *J. Mater. Chem. A* **2015**, *3* (35), 18163−18170.
(11) Kim, J. S.; Kim, T. G.; Kong, W. H.; Park, T. G.; Nam, Y. S. Thermally Controlled Wettability of a Nanoporous Membrane Grafted with Catechol-Tethered Poly(N-Isopropylacrylamide). *Chem. Commun.* **2012**, *48*, 9227−9229.
(12) Hong, C. A.; Son, H. Y.; Nam, Y. S. Layer-by-Layer SiRNA/Poly(L-Lysine) Multilayers on Polydopamine-Coated Surface for Efficient Cell Adhesion and Gene Silencing. *Sci. Rep.* **2018**, *8*, 7738−7745.
(13) Hong, S.; Lee, J. S.; Ryu, J.; Lee, S. H.; Lee, D. Y.; Kim, D.-P.; Park, C. B.; Lee, H. Bio-Inspired Strategy for on-Surface Synthesis of Silver Nanoparticles for Metal/Organic Hybrid Nanomaterials and LDI-MS Substrates. *Nanotechnology* **2011**, *22* (49), 494020−494027.
(14) Son, H. Y.; Kim, I.; Nam, Y. S. On-Surface Synthesis of Metal Nanostructures on Solid and Hydrated Polymer Nanofibers Coated with Polydopamine. *J. Ind. Eng. Chem.* **2015**, *30*, 220−224.
(15) Son, H. Y.; Kim, K. R.; Lee, J. B.; Le Kim, T. H.; Jang, J.; Kim, S. J.; Yoon, M. S.; Kim, J. W.; Nam, Y. S. Bioinspired Synthesis of Mesoporous Gold-Silica Hybrid Microspheres as Recyclable Colloidal SERS Substrates. *Sci. Rep.* **2017**, *7*, 14728−14741.
(16) Steenken, S.; Neta, P. One-Electron Redox Potentials of Phenols. Hydroxy- and Aminophenols and Related Compounds of Biological Interest. *J. Phys. Chem.* **1982**, *86* (18), 3661−3667.
(17) Lee, Y.; Park, T. G. Facile Fabrication of Branched Gold Nanoparticles by Reductive Hydroxyphenol Derivatives. *Langmuir* **2011**, *27* (6), 2965−2971.
(18) Son, H. Y.; Ryu, J. H.; Lee, H.; Nam, Y. S. Silver-Polydopamine Hybrid Coatings of Electrospun Poly(Vinyl Alcohol) Nanofibers. *Macromol. Mater. Eng.* **2013**, *298* (5), 547−554.
(19) Son, H. Y.; Lee, D. J.; Lee, J. B.; Park, C. H.; Seo, M.; Jang, J.; Kim, S. J.; Yoon, M. S.; Nam, Y. S. In Situ Functionalization of Highly Porous Polymer Microspheres with Silver Nanoparticles via Bio-Inspired Chemistry. *RSC Adv.* **2014**, *4* (98), 55604−55609.
(20) Wan, H.; Zou, Q.; Yan, R.; Zhao, F.; Zeng, B. Electrochemistry and Voltammetric Determination of Tannic Acid on a Single-Wall Carbon Nanotube-Coated Glassy Carbon Electrode. *Microchim. Acta* **2007**, *159* (1−2), 109−115.
(21) Çakar, S.; Güy, N.; Özacar, M.; Findik, F. Investigation of Vegetable Tannins and Their Iron Complex Dyes for Dye Sensitized Solar Cell Applications. *Electrochim. Acta* **2016**, *209*, 407−422.
(22) Tennakone, K.; Kumara, G. R. R. A.; Kumarasinghe, A. R.; Sirimanne, P. M.; Wijayantha, K. G. U. Efficient Photosensitization of Nanocrystalline TiO2 Films by Tannins and Related Phenolic Substances. *J. Photochem. Photobiol., A* **1996**, *94* (2−3), 217−220.
(23) McGilvray, K. L.; Granger, J.; Correia, M.; Banks, J. T.; Scaiano, J. C. Opportunistic Use of Tetrachloroaurate Photolysis in the Generation of Reductive Species for the Production of Gold Nanostructures. *Phys. Chem. Chem. Phys.* **2011**, *13*, 11914−11918.
(24) Son, H. Y.; Jun, H.; Kim, K. R.; Hong, C. A.; Nam, Y. S. Tannin-Mediated Assembly of Gold-Titanium Oxide Hybrid Nanoparticles for Plasmonic Photochemical Applications. *J. Ind. Eng. Chem.* **2018**, *63*, 420−425.
(25) Lee, J. B.; Choi, S.; Kim, J.; Nam, Y. S. Plasmonically-Assisted Nanoarchitectures for Solar Water Splitting: Obstacles and Breakthroughs. *Nano Today* **2017**, *16*, 61−81.
(26) Jun, H.; Choi, S.; Yang, M. Y.; Nam, Y. S. A Ruthenium-Based Plasmonic Hybrid Photocatalyst for Aqueous Carbon Dioxide Conversion with a High Reaction Rate and Selectivity. *J. Mater. Chem. A* **2019**, *7* (29), 17254−17260.
(27) Kim, J.; Kim, K. R.; Hong, Y.; Choi, S.; Yavuz, C. T.; Kim, J. W.; Nam, Y. S. Photochemically Enhanced Selective Adsorption of Gold Ions on Tannin-Coated Porous Polymer Microspheres. *ACS Appl. Mater. Interfaces* **2019**, *11* (24), 21915−21925.
(28) Jin, J.; Yu, J.; Guo, D.; Cui, C.; Ho, W. A Hierarchical Z-Scheme CdS-WO3 Photocatalyst with Enhanced CO2 Reduction Activity. *Small* **2015**, *11* (39), 5262−5271.
(29) Di, T.; Zhu, B.; Cheng, B.; Yu, J.; Xu, J. A Direct Z-Scheme g-C3N4/SnS2 Photocatalyst with Superior Visible-Light CO2 Reduction Performance. *J. Catal.* **2017**, *352*, 532−541.
(30) Fujishima, A.; Honda, K. Electrochemical Photolysis of Water at a Semiconductor Electrode. *Nature* **1972**, *238* (5358), 37−38.
(31) Schneider, J.; Matsuoka, M.; Takeuchi, M.; Zhang, J.; Horiuchi, Y.; Anpo, M.; Bahnemann, D. W. Understanding TiO2 Photocatalysis: Mechanisms and Materials. *Chem. Rev.* **2014**, *114* (19), 9919−9986.
(32) Son, H. Y.; Koo, B. Il; Lee, J. B.; Kim, K. R.; Kim, W.; Jang, J.; Yoon, M. S.; Cho, J. W.; Nam, Y. S. Tannin-Titanium Oxide Multilayer as a Photochemically Suppressed Ultraviolet Filter. *ACS Appl. Mater. Interfaces* **2018**, *10*, 27344−27354.
(33) Park, J. Y.; Yeom, J.; Kim, J. S.; Lee, M.; Lee, H.; Nam, Y. S. Cell-Repellant Dextran Coatings of Porous Titania Using Mussel Adhesion Chemistry. *Macromol. Biosci.* **2013**, *13*, 1511−1519.
(34) Li, H.; Tu, W.; Zhou, Y.; Zou, Z. Z-Scheme Photocatalytic Systems for Promoting Photocatalytic Performance: Recent Progress and Future Challenges. *Adv. Sci.* **2016**, *3* (11), 1500389−1500401.
(35) Brunauer, S.; Deming, L. S.; Deming, W. E.; Teller, E. Adsorption of Gases in Multimolecular Layers. *J. Am. Chem. Soc.* **1940**, *62*, 1723−1732.
(36) Liu, Y.; Shen, L. From Langmuir Kinetics to First- and Second-Order Rate Equations for Adsorption. *Langmuir* **2008**, *24*, 11625−11630.
(37) Rudzinski, W.; Plazinski, W. Kinetics of Solute Adsorption at Solid/Solution Interfaces: A Theoretical Development of the Empirical Pseudo-First and Pseudo-Second Order Kinetic Rate Equations, Based on Applying the Statistical Rate Theory of Interfacial Transport. *J. Phys. Chem. B* **2006**, *110*, 16514−16525.
(38) Foo, K. Y.; Hameed, B. H. Insights into the Modeling of Adsorption Isotherm Systems. *Chem. Eng. J.* **2010**, *156*, 2−10.
(39) Lee, H.; Dellatore, S. M.; Miller, W. M.; Messersmith, P. B. Mussel-Inspired Surface Chemistry for Multifunctional Coatings. *Science (Washington, DC, U. S.)* **2007**, *318* (5849), 426−430.
(40) Zhang, L.; Li, Z.; Du, X.; Chang, X. Activated Carbon Functionalized with 1-Amino-2-Naphthol-4-Sulfonate as a Selective Solid-Phase Sorbent for the Extraction of Gold(III). *Microchim. Acta* **2011**, *174* (3), 391−398.
(41) Li, D.; Chang, X.; Hu, Z.; Wang, Q.; Tu, Z.; Li, R. Selective Solid-Phase Extraction of Trace Au(III), Pd(II) and Pt(IV) Using Activated Carbon Modified with 2,6-Diaminopyridine. *Microchim. Acta* **2011**, *174* (1), 131−136.
(42) Shaheen, H. A.; Marwani, H. M.; Soliman, E. M. Selective Adsorption of Gold Ions from Complex System Using Oxidized Multi-Walled Carbon Nanotubes. *J. Mol. Liq.* **2015**, *212*, 480−486.
(43) Guin, P. S.; Das, S.; Mandal, P. C. Electrochemical Reduction of Quinones in Different Media: A Review. *Int. J. Electrochem.* **2011**, *2011*, 1−22.
(44) Novak, I.; Šeruga, M.; Komorsky-Lovrić, Š. Electrochemical Characterization of Epigallocatechin Gallate Using Square-Wave Voltammetry. *Electroanalysis* **2009**, *21*, 1019−1025.
(45) Patil, N.; Jérôme, C.; Detrembleur, C. Recent Advances in the Synthesis of Catechol-Derived (Bio)Polymers for Applications in Energy Storage and Environment. *Prog. Polym. Sci.* **2018**, *82*, 34−91.
(46) Paul, K. K.; Giri, P. K. Role of Surface Plasmons and Hot Electrons on the Multi-Step Photocatalytic Decay by Defect Enriched Ag@TiO2 Nanorods under Visible Light. *J. Phys. Chem. C* **2017**, *121* (36), 20016−20030.
(47) Guo, H. L.; Du, H.; Jiang, Y. F.; Jiang, N.; Shen, C. C.; Zhou, X.; Liu, Y. N.; Xu, A. W. Artificial Photosynthetic Z-Scheme

https://dx.doi.org/10.1021/acssuschemeng.0c00860
ACS Sustainable Chem. Eng. 2020, 8, 7359−7370

Photocatalyst for Hydrogen Evolution with High Quantum Efficiency. *J. Phys. Chem. C* **2017**, *121* (1), 107−114.
(48) Wu, Z.; Yuan, W.; Li, J.; Wang, X.; Liu, L.; Wang, J. A Critical Review on the Recycling of Copper and Precious Metals from Waste Printed Circuit Boards Using Hydrometallurgy. *Front. Environ. Sci. Eng.* **2017**, *11*, 8−22.
(49) Jing-Ying, L.; Xiu-Li, X.; Wen-Quan, L. Thiourea Leaching Gold and Silver from the Printed Circuit Boards of Waste Mobile Phones. *Waste Manage.* **2012**, *32*, 1209−1212.
(50) Adhikari, B. B.; Gurung, M.; Alam, S.; Tolnai, B.; Inoue, K. Kraft Mill Lignin - A Potential Source of Bio-Adsorbents for Gold Recovery from Acidic Chloride Solution. *Chem. Eng. J.* **2013**, *231*, 190−197.
(51) Kvítek, L.; Prucek, R.; Panáček, A.; Novotný, R.; Hrbáč, J.; Zbořil, R. The Influence of Complexing Agent Concentration on Particle Size in the Process of SERS Active Silver Colloid Synthesis. *J. Mater. Chem.* **2005**, *15*, 1099−1105.
(52) Cleare, M. J.; Charlesworth, P.; Bryson, D. J. Solvent Extraction in Platinum Group Metal Processing. *J. Chem. Technol. Biotechnol.* **1979**, *29*, 210−224.
(53) Gurung, M.; Adhikari, B. B.; Kawakita, H.; Ohto, K.; Inoue, K.; Alam, S. Recovery of Au(III) by Using Low Cost Adsorbent Prepared from Persimmon Tannin Extract. *Chem. Eng. J.* **2011**, *174*, 556−563.
(54) Guo, J.; Ping, Y.; Ejima, H.; Alt, K.; Meissner, M.; Richardson, J. J.; Yan, Y.; Peter, K.; Von Elverfeldt, D.; Hagemeyer, C. E.; Caruso, F. Engineering Multifunctional Capsules through the Assembly of Metal-Phenolic Networks. *Angew. Chem., Int. Ed.* **2014**, *53* (22), 5546−5551.
(55) Chen, X.; Lam, K. F.; Mak, S. F.; Yeung, K. L. Precious Metal Recovery by Selective Adsorption Using Biosorbents. *J. Hazard. Mater.* **2011**, *186* (1), 902−910.

https://dx.doi.org/10.1021/acssuschemeng.0c00860
ACS Sustainable Chem. Eng. 2020, 8, 7359−7370